Journal of The Electrochemical Society, **158** (1) H1-H4 (2011)
0013-4651/2010/158(1)/H1/4/$28.00 © The Electrochemical Society

Etching of CoFeB Using CO/NH_3 in an Inductively Coupled Plasma Etching System

Jong-Yoon Park,[a] Se-Koo Kang,[a] Min-Hwan Jeon,[a] Myung S. Jhon,[c] and Geun-Young Yeom[a,b,z]

[a]*Sungkyunkwan University Advanced Institute of Nano Technology, and* [b]*Department of Advanced Materials Science and Engineering, Sungkyunkwan University, Suwon, Gyeonggi-do 440-746, Korea*
[c]*Department of Chemical Engineering, Carnegie Mellon University, Pittsburgh, Pennsylvania 15213, USA*

A CoFeB thin film composing a magnetic tunneling junction of CoFeB/MgO/CoFeB was etched in an inductively coupled plasma (ICP) etching system using CO/NH_3 gas mixtures, and its etch characteristics were compared with those of the CoFeB thin film etched using Cl_2/Ar. When Cl_2/Ar was used to etch the CoFeB thin film, even though its etch rate was faster than that of the CoFeB thin film etched using CO/NH_3, a rough CoFeB surface could be observed due to the corrosion of the CoFeB surface during exposure to the air in addition to the significant change of surface composition. On the other hand, no corrosion of the CoFeB thin film was observed after the etching using CO/NH_3. When the ratio of CO/NH_3 was varied, the highest etch rate of 12 nm/min could be observed at the ratio of 1:3 compared to about 4 nm/min for CO or NH_3 at the ICP source power of 700 W, bias power of 300 W, and 5 mTorr of operating pressure. The highest etch rate was related to the formation of volatile metal carbonyls between metal and CO, where NH_3 appeared to assist the easier formation of metal carbonyl by preventing the dissociation of CO into C and CO_2.
 [DOI: 10.1149/1.3505295]

Manuscript submitted June 24, 2010; revised manuscript received October 4, 2010. Published November 10, 2010.

Magnetic random access memory (MRAM) devices have fast access time, high storage densities, radiation harness, and infinite rewrite capability in contrast to conventional memory devices. MRAM, a nonvolatile memory device with low power consumption, is being investigated as one of the most suitable alternatives for the next generation memory devices. Among the MRAMs, spin-transfer-torque (STT)-MRAM has the characteristics that are applicable to highly integrated circuit because of the lower required current density in the operation of the device. For STT-MRAM, ferromagnetic layers such as CoFeB/MgO/CoFeB are used as the magnetic tunneling junction (MTJ) layer.[1] The MTJ layer composed of CoFeB/MgO/CoFeB is also used as a key element of advanced spintronic devices such as magnetic read heads for ultra-high-density hard disk drives in addition to the high-capacity non-volatile-MRAMs.[2]

For the processing of the MRAMs, the dry etch process is one of the important issues due to the difficulty in the formation of volatile compounds between the ferromagnetic materials such as Ni, Fe, and Co and etching gases. Recently, Arion milling has been successfully applied to the fabrication of the device, although the redeposition of the back-sputtered etch products on the sidewalls and the low etch rate are the main disadvantages of this method. The etch rates higher than 50 Å/s for magnetic multilayer structures using Cl_2/Ar plasmas are also reported using conventional reactive ion etching techniques; however, these processes tend to show problems due to nonvolatile products remaining on the sidewalls of the device and the corrosion caused by residual chlorine.[3-7] As a result, for the minimization of the corrosion after the etching in addition to the formation of volatile etch products, etching chemistries which may form volatile metal organic gases with magnetic materials such as CO/NH_3, and CH_3OH have been investigated in the recent researches.[2,8-14] For example, Otani et al.[2] reported the successful etching of the 100-nm-scale CoFeB/MgO/CoFeB MTJs using a CH_3OH etching process in an inductively coupled plasma (ICP) etching system. Nakatani et al.[15] also reported the etching of NiFe and NiFeCo using noncorrosive CO/NH_3 gases in a capacitively coupled plasma etching system. In their researches, an increase was observed in the etch rate of NiFe and NiFeCo for about five times by the addition of 50% NH_3 to CO.

It is believed that the gas combination of CO/NH_3 can also be applied to the etching of the MTJ layer composed of CoFeB/MgO/CoFeB by forming volatile metal organic gases similar to CH_3OH, even though no research on the etching of CoFeB/MgO/CoFeB using a CO/NH_3 gas combination has been reported. Therefore, in this study, the magnetic layers such as CoFeB, and MgO composing the MTJ layer were etched using CO/NH_3 gas combination in an ICP system and their etch characteristics were investigated.

Experimental

The etch system used in the experiment is shown in Fig. 1. The etch system was a commercial ICP etching system (STS PLC, UK) with a load lock. As shown in the figure, one-turn inductive coil was wound around the ceramic chamber wall for the inductive coupling to the plasma and 13.56 MHz rf power was applied to the coil. The substrate size was 8 in. diameter, and a 13.56 MHz rf power was also applied to the substrate for the rf biasing. During the processing, the substrate was cooled to about 40–50°C by He cooling.

CoFeB, a magnetic material of the MTJ layer composed of CoFeB/MgO/CoFeB, was used as the sample to be etched, and other materials forming the MRAM, such as MgO and Ti (etch mask of MTJ layer), were also etched and their etch characteristics were compared. These materials were prepared by a cosputter deposition technique. Cl_2/Ar and the CO/NH_3 gas mixtures were used to etch

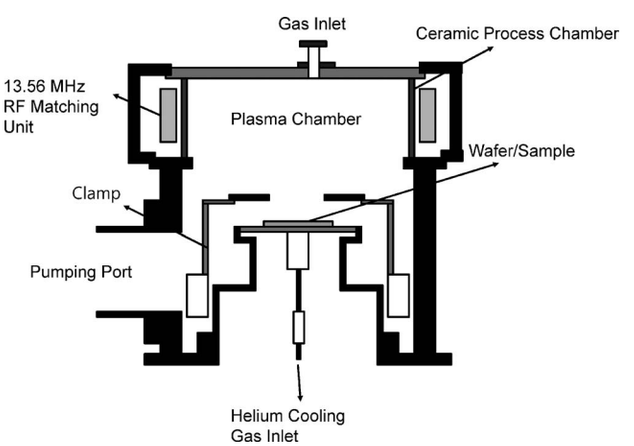

Figure 1. Schematic diagram of the inductively coupled plasma etching system used in the experiment.

[z] E-mail: gyyeom@skku.edu

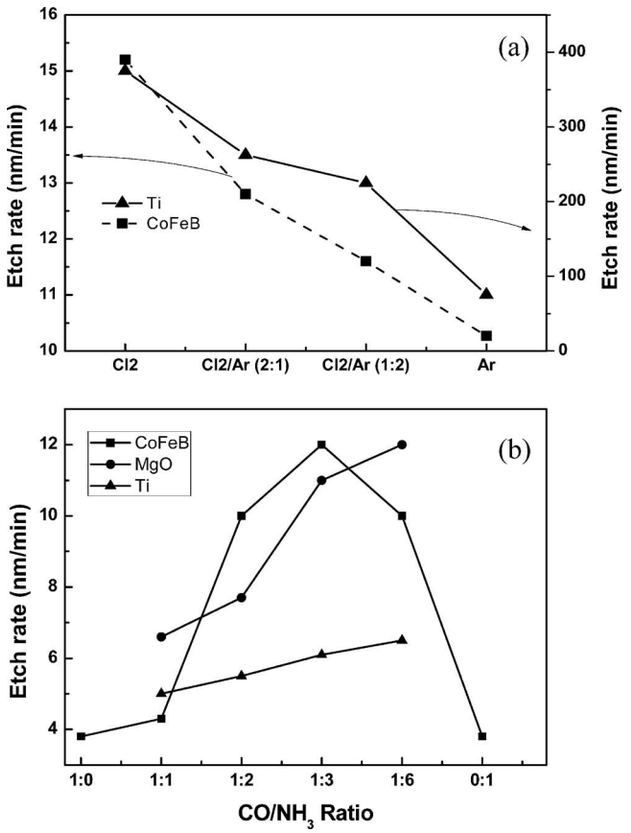

Figure 2. Etch rates of CoFeB and Ti as a function of (a) Cl_2/Ar gas ratio and (b) CO/NH_3 gas ratio. MgO etch rate as a function of CO/NH_3 gas ratio is also shown.

the materials. The ICP source power of 700 W and the bias power of 300 W were applied to etch CoFeB. The operating pressure was fixed at 5 mTorr with 50 sccm of gas flow rate.

Secondary electron microscopy (SEM, Hitachi S-4700) was used to examine the surface of the etched CoFeB, and a step profilometer (Alpha step 500, Tencor) was used to measure the etch rate. X-ray photoelectron spectroscopy (XPS, ESCA2000, VG Microtech Inc.) was used to investigate the binding states and the residue remaining on the etched magnetic material surface.

Results and Discussion

Figure 2a shows the etch rates of CoFeB and Ti measured as a function of the Cl_2/Ar gas mixture using the ICP etching system. The ICP source power and the bias power were maintained at 700 and 300 W, respectively. The operating pressure and the total flow rate of the Cl_2/Ar gas mixture were fixed at 5 mTorr and 50 sccm, respectively. As shown in the figure, the Ti etch rate significantly increased with the increase of Cl_2 percentage in the Cl_2/Ar gas mixture from 20 nm/min for pure Ar to 400 nm/min for pure Cl_2 while the etch rate of CoFeB increased moderately with the increase of Cl_2 percentage in the Cl_2/Ar gas mixture from about 11 nm/min for pure Ar to 15 nm/min for pure Cl_2. In Table I, the boiling points of the possible etch by-products formed during the etching of CoFeB and Ti with Cl_2/Ar are shown.[16] As shown, the boiling point of Ti chloride is lower than that of Co chlorides and Fe chlorides in CoFeB, possibly indicating higher vapor pressure. Therefore, it is believed that Ti showed a much higher etch rate at a fixed Cl_2/Ar gas mixture compared to CoFeB.[17] Both Ti and CoFeB showed the increased etch rate with the increase of Cl_2 percentage in the Cl_2/Ar gas mixture due to the higher removal rate of the chlorides compared to sputtering.

Table I. Boiling points of reaction products of Co/Fe/B and Ti with Cl_2 and CO/NH_3.[16]

		Cl_2	
	CO/NH_3	100 kPa	10 kPa
Co	$Co_2(CO)_8$:52°C	$CoCl_2$:1049°C	$CoCl_2$:818°C
Fe	$Fe(CO)_5$:103°C	$FeCl_2$:1025°C	$FeCl_2$:821°C
		$FeCl_3$:315°C	$FeCl_3$:268°C
B	B_2H_6:−92.6°C	BCl_3:12.5°C	BCl_3:−93°C
Ti		$TiCl_4$:136°C	

CoFeB and Ti were also etched using CO/NH_3 gas mixtures instead of Cl_2/Ar gas mixtures, and the results are shown in Fig. 2b. The ICP power, bias power, operating pressure, and gas flow rates were maintained at the same conditions as in Fig. 2a. In Fig. 2b, the MgO etch rate is also shown. In Fig. 2b, the etch rate of CoFeB is shown to be a maximum of 12 nm/min at the CO/NH_3 gas mixture ratio of 1:3 while the etch rate for both pure CO and pure NH_3 is about 4 nm/min. Therefore, about three times higher etch rate could be achieved by using the CO/NH_3 gas mixture instead of pure gases. The etch rate of MgO at the CO/NH_3 gas mixture ratio also appeared to follow that of CoFeB by showing a higher etch rate of 11 nm/min at the CO/NH_3 gas mixture ratio of 1:3 compared to about 6 nm/min at the CO/NH_3 gas mixture ratio of 1:1. However, in the case of Ti, no significant change of etch rate was observed with the change of CO/NH_3 gas mixture ratio. When Ni, Co, or Fe is etched using CO/NH_3, it is known that these metals form metal carbonyls such as $Ni(CO)_4$, $Co_2(CO)_8$, and $Fe(CO)_5$ by the recombination of CO with these metals.

In Table I, the boiling points of Fe carbonyls and Co carbonyls are also shown and, as shown in Table I, due to the boiling points of these metal carbonyls such as 52°C for $Co_2(CO)_8$ and 103°C for $Fe(CO)_5$, low vapor pressures of these metal carbonyls are also expected. Therefore, high etch rates of CoFeB can be obtained by the formation of metal carbonyls during the etching of CoFeB using CO/NH_3. However, CO is known to spontaneously decompose into C and CO_2 on the surface by the equation[15]

$$2CO \rightarrow C + CO_2\ ; \quad \Delta H^\circ = -172.5\ \text{kJ/mol} \qquad [1]$$

Therefore, by the decomposition of CO into C and CO_2, the portion of chemical etching is decreased and the material is etched mostly by physical sputtering, which results in the decrease of the etch rate. The decomposition of CO in the plasma is known to be decreased by the addition of NH_3 in the plasma.[15] Therefore, the highest etch rate obtained with the CO/NH_3 ratio of 1:3 in Fig. 2b is believed to be related to the abundance of CO on the metal surface, which results in the formation of volatile metal carbonyls. In the case of MgO, even though it is not clear, Mg appears to form volatile metal carbonyls with CO; therefore, a similar increase of the etch rate is obtained at the CO/NH_3 ratio of 1:3. However, in the case of Ti, no such volatile metal carbonyls appear to form; therefore, the etch rate was not affected by the ratio of CO/NH_3 because the etching is obtained by the physical sputtering.

By using CO/NH_3 (1:3) instead of Cl_2/Ar (2:1) for the etching of CoFeB, even though the CoFeB etch rate is slightly decreased, the etch selectivity over Ti, which is the mask for the MTJ layer, is significantly increased from 0.068 for Cl_2/Ar (2:1) to 2.0 for CO/NH_3 (1:3) as shown in Fig. 2a and b, respectively. More important factor is the corrosion after the etching of CoFeB. Figure 3 shows the SEM micrographs after the etching using Cl_2/Ar (2:1) and CO/NH_3 (1:3), respectively. The ICP source power, bias power, operating pressure, and gas flow rate were maintained at 700 W, 500 W, 5 mTorr, and 30 sccm, respectively. The etch time of CoFeB was 1 min. As shown in Fig. 3, for the CoFeB etched by Cl_2/Ar, a rough surface caused by the surface corrosion by the remaining Cl_2 could be observed as similarly observed by other

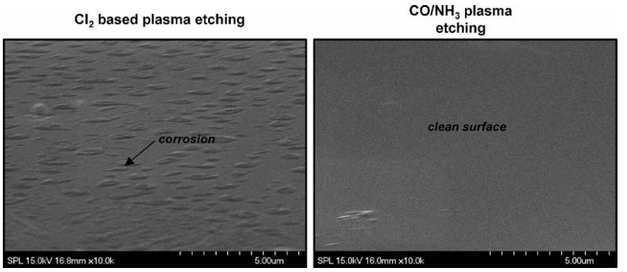

Figure 3. SEM images of CoFeB surface after the etching by Cl_2/Ar (2:1) and CO/NH_3 (1:3).

researchers,[12] while a smooth surface was obtained for the CoFeB etched by CO/NH_3 due to no corrosion behavior. Also, the etch rate of MgO similar to that of CoFeB with CO/NH_3 (1:3) appears to be beneficial in the one step etching of the MTJ layer composed of CoFeB/MgO/CoFeB.

The CoFeB surfaces etched by Cl_2/Ar (2:1) and CO/NH_3 (1:3) shown in Fig. 3 were further investigated using XPS. Figure 4 shows the XPS narrow scan data of Fe 2*p*, Co 2*p*, and B 1*s* for the CoFeB etched by Cl_2/Ar (2:1) and CO/NH_3 (1:3). The etch conditions are the same as shown for Fig. 3. The XPS data of Co, Fe, and B for the pristine CoFeB were also taken as references. The etched CoFeB surface was in situ sputtered for XPS depth profiling by Ar^+ ion gun with the ion energy of 2 kV and the ion current of 2 μA. XPS data were taken again after the sputtering of the surface for 120 s/cycle. For the pristine CoFeB, to expose clean surface, XPS data were taken after the sputtering for 6 min (three cycles). As shown in Fig. 4, the composition ratio of Co: Fe: B for the pristine CoFeB measured by XPS was about 54%:34%:12%. Also, as shown in Fig. 4, on the surface of the CoFeB etched by Cl_2/Ar, the XPS peaks possibly related to chlorides are observed at 780.5 eV for Co 2*p*, 711.0 eV for Fe 2*p*, and 192.6 eV for B 1*s* because it is known that Co 2*p* peak related to $CoCl_2$(MO) is observed at 780–782 eV, Fe 2*p* peaks related to $FeCl_2$ and $FeCl_3$ are observed at 710.6 and 711.3 eV, respectively, and B 1*s* peak related to BCl_3(MO) are observed at 192.6–192.7 eV.[18-20] After the sputtering of the etched surface for more than 120 s (one cycle), the peak heights related to chlorides decrease and the peaks related to the metallic binding among Co, Fe, and B emerge at the binding peak energies for the pristine CoFeB, indicating a thick chloride layer on the CoFeB

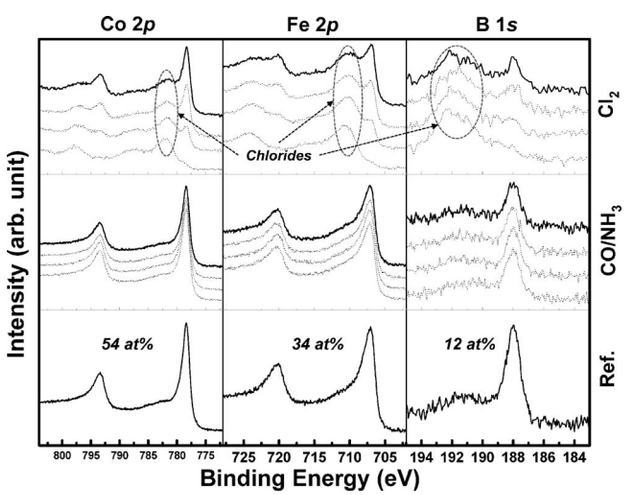

Figure 4. XPS narrow scan data of Co, Fe, and B on the surface of CoFeB etched with Cl_2/Ar (2:1) and CO/NH_3 (1:3). XPS narrow scan data of pristine CoFeB is also shown.

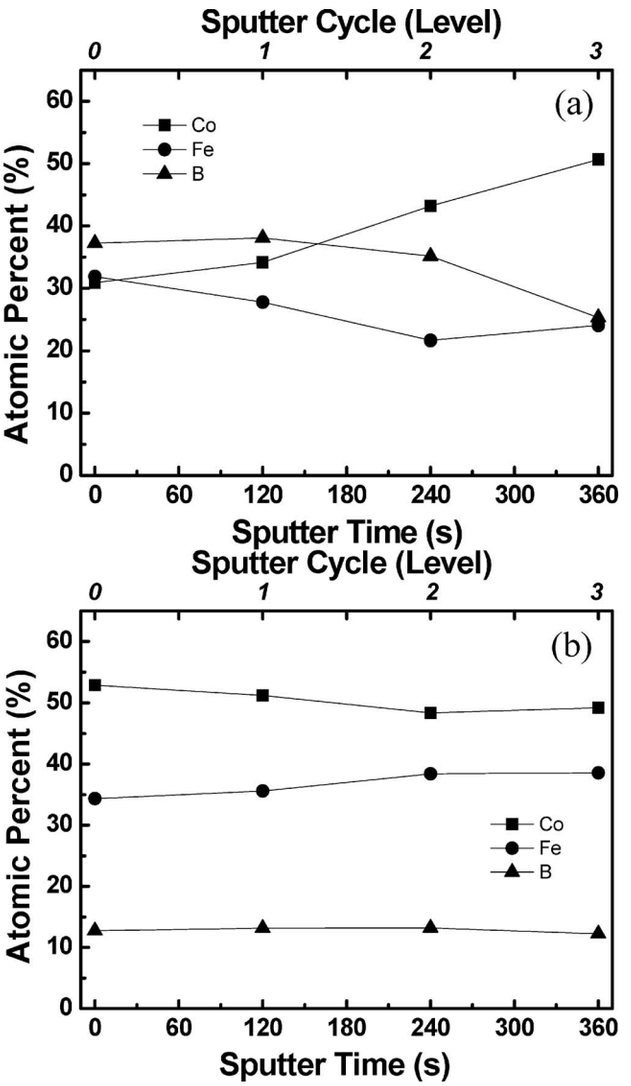

Figure 5. Reative atomic percentage of the etched CoFeB measured as a function of Ar^+ ion sputter time for the CoFeB samples etched by (a) Cl_2/Ar and (b) CO/NH_3.

etched by Cl_2/Ar. However, in the case of the CoFeB etched by CO/NH_3, the XPS peaks related to the pristine CoFeB were observed even before the sputtering and no other peaks were observed after the sputtering. Therefore, the CoFeB etched by CO/NH_3 showed a clean surface close to that of the pristine CoFeB, while the CoFeB etched by Cl_2/Ar showed a thick chloride layer on the etched CoFeB surface.

The change of relative CoFeB composition ratio of the etched CoFeB surface as a function of Ar^+ ion sputter time was measured for the CoFeB samples etched by Cl_2/Ar and CO/NH_3, and the results are shown in Fig. 5a for the CoFeB etched by Cl_2/Ar and in Fig. 5b for the CoFeB etched by CO/NH_3. The etch conditions were the same as those in Fig. 3. As shown in the figure, in the case of the CoFeB etched by Cl_2/Ar, the composition ratio of CoFeB has changed significantly by showing boron-rich surface. The boron-rich composition ratio of the CoFeB etched by Cl_2/Ar remained similar for the sputter time of 360 s, indicating the formation of a thick degraded layer on the surface. However, in the case of the CoFeB etched by CO/NH_3, the composition ratio of on the etched CoFeB was similar to that of the pristine CoFeB and the composition re-

mained similar with the increase of sputter time; therefore, no significant change of the surface composition ratio of the CoFeB occurred by the etching with CO/NH_3.

Conclusions

In this study, CoFeB, which is used as the MTJ layer for MRAM, and the other materials such as Ti and MgO related to the MTJ layer were etched using CO/NH_3 ICP and the etch characteristics were compared with the CoFeB etched using Cl_2/Ar ICP.

When CoFeB was etched using Cl_2/Ar ICP, the etch rate of CoFeB increased with the increase of Cl_2 percentage in Cl_2/Ar possibly due to the formation of more volatile chlorides on the surface; however, the CoFeB etched by Cl_2/Ar showed the corrosion on the etched surface, lower etch selectivity to the Ti mask layer by showing etch selectivity of CoFeB to Ti less than 0.1, and a thick degraded surface layer. When CO/NH_3 gas mixtures were used, the highest etch rate was obtained at the CO/NH_3 gas ratio of 1:3. The highest CoFeB etch rate obtained at the CO/NH_3 ratio of 1:3 is believed to be related to the prevention of CO decomposition into C and CO_2 by the addition of NH_3 and the formation of more volatile metal carbonyls. When CO/NH_3 gas mixtures were used instead of Cl_2/Ar, even though the etch rate is a little lower, no corrosion on the etched surface, higher etch selectivity to Ti close to 2.0, and no formation of noticeable degraded surface layer could be observed. In addition, by using CO/NH_3, the MTJ layer can be etched by one step etching by showing the MgO etch rate similar to the etch rate of CoFeB.

Acknowledgments

This work was supported by the IT R&D program of MKE/KEIT (2009-F-004-01, Technology Development of 30 nm level High Density Perpendicular STT-MRAM), and by the World Class University program (grant no. R32-2008-000-10124-0) and Basic Science Research program (2010-0015035) of National Research Foundation of Korea.

Sungkyunkwan University assisted in meeting the publication costs of this article.

References

1. D. D. Djayaprawira, K. Tsunekawa, M. Nagai, H. Maehara, S. Yamagata, N. Watanabe, S. Yuasa, and K. Ando, *Appl. Phys. Lett.*, **86**, 092502 (2005).
2. Y. Otani, H. Kubota, A. Fukushima, H. Maehara, T. Osada, S. Yuasa, and K. Ando, *IEEE Trans. Magn.*, **43**, 2776 (2007).
3. K. Kinoshita, K. Yamada, and H. Matsutera, *IEEE Trans. Magn.*, **27**, 4888 (1990).
4. K. Ichihara and M. Hara, *Jpn. J. Appl. Phys., Part 1*, **36**, 4874 (1997).
5. K. B. Jung, E. S. Lambers, J. R. Childress, S. J. Pearton, M. Jeason, and A. T. Hurst, Jr., *J. Vac. Sci. Technol. A*, **16**, 23 (1998).
6. M. J. Vasile and C. J. Mogab, *J. Vac. Sci. Technol. A*, **4**, 1841 (1986).
7. X. Peng, S. Wakeham, A. Morrone, S. Axdal, M. Feldbaum, J. Hwu, T. Boonstra, Y. Chen, and J. Ding, *Vacuum*, **83**, 1007 (2009).
8. K. B. Jung, J. Hong, H. Cho, S. Onishi, D. Johnson, Y. D. Park, J. R. Childress, and S. J. Pearton, *J. Electrochem. Soc.*, **146**, 2163 (1999).
9. N. Matsui, K. Mashimo, A. Egami, A. Konishi, O. Okada, and T. Tsukada, *Vacuum*, **66**, 479 (2002).
10. H. Kubota, K. Ueda, Y. Ando, and T. Miyazaki, *J. Magn. Magn. Mater.*, **272–276**, e1421 (2004).
11. A. S. Orland and R. Blumenthal, *J. Vac. Sci. Technol. B*, **23**, 1597 (2005).
12. X. Kong, D. Krasa, H. P. Zhou, W. Williams, S. McVitie, J. M. R. Weaver, and C. D. W. Wilkinson, *Microelectron. Eng.*, **85**, 988 (2008).
13. K. B. Jung, H. Cho, K. P. Lee, and S. J. Pearton, *J. Vac. Sci. Technol. B*, **17**, 3186 (1999).
14. S. J. Pearton, H. Cho, K. B. Jung, J. R. Childress, F. Sharifi, and J. Marburger, *Mater. Res. Soc. Symp. Proc.*, **614**, F10.2.1 (2000).
15. I. Nakatani, *IEEE Trans. Magn.*, **32**, 4448 (1996).
16. D. R. Lide, *Handbook of Chemistry and Physics*, 84th ed., CRC Press, Boca Raton, FL (2004).
17. H. N. Cho, S. R. Min, H. J. Bae, J. H. Lee, and C. W. Jung, *J. Ind. Eng. Chem. (Seoul, Repub. Korea)*, **13**, 939 (2007).
18. A. Thompson, I. Lindau, D. Attwood, P. Pianetta, E. Gullikson, A. Robinson, M. Howells, J. Scofield, K.-J. Kim, J. Underwood, et al., *Ray Data Booklet*, 2nd ed., Lawrence Berkeley National Laboratory (2001).
19. J. F. Moulder, W. F. Stickle, P. E. Sobol, and K. D. Bomben, *Handbook of X-Ray Photoelectron Spectroscopy* (1992).
20. A. Kikas, R. Ruus, A. Saar, E. Nommiste, T. Kaambre, and S. Sundin, *J. Electron Spectrosc. Relat. Phenom.*, **101–103**, 745 (1999).